# Aberration characterisation in coherent Fourier scatterometry

Sarika Soman and Silvania F. Pereira

Delft University of Technology, Department of Imaging Physics
Lorentzweg 1, 2628 CJ, Delft, The Netherlands

## ABSTRACT

Coherent Fourier scatterometry (CFS) is a very sensitive optical metrology technique that has been applied for detection and characterisation of nanostructures. It is a scanning-based technique where the samplie is illuminated with a focused light spot. However, in practical CFS systems, residual optical aberrations can distort the focused spot and degrade the signal-to-noise ratio during measurements. Here, we present a systematic study of the influence of low-order aberrations: defocus, spherical, astigmatism, oblique astigmatism, and coma on the differential split-detector CFS signal. Controlled amounts of each aberration, described by Zernike polynomials, were introduced into the Fourier plane via a spatial light modulator. Two-dimensional differential scattering maps were recorded on a reference sample of 425 nm diameter, 150 nm deep pits etched in silicon, and the peak-to-peak differential signal was quantified as a function of peak-valley (PV) wavefront error. We find that defocus has the strongest impact, halving the signal at just $0.27\lambda$ PV, followed by spherical ($0.32\lambda$) and coma ($0.40\lambda$), whereas astigmatism and oblique astigmatism require larger wavefront errors ($> 0.6\lambda$) to produce comparable signal loss. These results define quantitative aberration tolerances for CFS systems. The insights gained here can guide the design and optimisation of different CFS implementations for in-line process control and nanostructure metrology.

**Keywords:** Coherent Fourier scatterometry, optical aberrations, Zernike polynomials, spatial light modulator, differential detection, nanometrology

## 1. INTRODUCTION

Scatterometry is a metrology technique used to characterise nanostructures primarily in the semiconductor industry.[1–4] It is a model-based technique and measures the scattering response from a sample at a single wavelength from multiple angles or multiple wavelengths at a single angle. The scattered field acts as a signature of the nanostructure and is used to infer its geometric parameters by solving an inverse problem. Coherent Fourier scatterometry (CFS) is an advanced scatterometry technique in which the scattering response from multiple angles is recorded simultaneously.[5] It uses an objective to focus the light from a collimated coherent laser source onto the sample. The scattered field after collection by the same objective is recorded using a detector placed in the Fourier plane. Each point in the Fourier plane corresponds to a distinct angle of incidence. The focused spot is scanned across the sample surface and the scattered field in the Fourier plane is recorded for each position. The use of a focused spot addresses one of the key limitations of regular scatterometry techniques, namely the limited spatial resolution. The high spatial resolution along with the capability to detect isolated nano-particles and characterise deep-subwavelength features of nanostructures make CFS a powerful tool. This technique has been successfully applied to a wide range of applications, including diffraction grating characterisation,[6] nerve crossing detection,[7] defect detection on SiC wafers for power electronics,[8] and nanoparticle characterization on Si wafers and plastic substrates.[9] For certain applications such as contamination detection, a two-pixel detector with differential detection was found to be a sufficient replacement for the multi-pixel CCD cameras, also enabling faster scanning. The differential detection enables the elimination of common mode noises and improves the signal-to-noise ratio (SNR). The differential detector along with 2D sample scanning is used to generate a 2D differential scattering map of the sample surface.

Further author information: (Send correspondence to S.S.)
S.S.: E-mail: s.soman@tudelft.nl
S.F.P.: E-mail: s.f.pereira@tudelft.nl

Optical Measurement Systems for Industrial Inspection XIV, edited by Peter Lehmann, Wolfgang Osten, Armando Albertazzi Gonçalves, Proc. of SPIE Vol. 13567, 135672J
2025 Published by SPIE · 0277-786X · doi: 10.1117/12.3062562

The scattering response is generated as a result of the interaction of the focused spot with the sample. In general, the detection limit of the system is assumed to be the random measurement noise generated from different sources, such as laser power fluctuations, electronic noise, and the surface roughness of the sample. In practice, the response is also affected by the inevitable optical aberrations present in the system. They can distort the intensity distribution of the focused spot in the focal plane and can vary the scattered field recorded at the Fourier plane.

In this work, we study the influence of different optical aberrations such as defocus, astigmatism, coma and spherical aberration on the CFS signal acquired using a two-pixel detector. Specific aberrations are introduced into the system using a spatial light modulator (SLM). The rest of the paper is structured as follows: section 2 details the CFS measurement principle, the description of optical aberrations using Zernike polynomials is described in section 3, the experimental setup used to introduce controlled aberrations is detailed in section 4 and their influence on the scan signal is presented in section 5 followed by a short discussion in section 6.

## 2. MEASUREMENT PRINCIPLE

CFS captures the angle-resolved scattering response of a sample in a single shot per position of the focused spot on the sample. A microscope objective transforms a collimated laser beam into a tightly focused spot on the surface. Each point in the Fourier plane, i.e. the back focal plane of the objective, corresponds to a distinct angle of incidence with the maximum angle limited by the objective numerical aperture (NA). The field after reflection from the sample is captured by the same objective and measured in the Fourier plane. Repeating this measurement while raster-scanning the focused spot across the surface yields a complete map of angle-resolved scattering for the entire surface. These measured fields serve as input to an inverse-scattering algorithm that retrieves the structural parameters of the sample.

Two complementary detection schemes are employed, depending on the application. A CCD camera records the full field intensity distribution across the Fourier plane and is preferred for reconstruction tasks such as grating profile determination or nanostructure shape retrieval. By contrast, a differential bi-cell detector integrates the intensity on two photodiodes and returns their electronic difference. This high-speed read-out is well suited to in-line process control, for example, contamination or overlay monitoring. In the differential scheme, the bicell produces zero signal when the focused spot illuminates a region with no nanostructures, because the Fourier-plane intensity distribution is symmetric. As the spot scans across a nanostructure, the scattering pattern becomes asymmetric, giving a non-zero differential signal.

Figure 1 shows an example of CFS measurement with the differential detection scheme. The sample consists of an etched pit of 425 nm diameter and 150 nm etch depth raster scanned using a focused spot generated using a 0.4 NA objective and HeNe laser (632.8 nm wavlength). Figure 1.a shows the 2D difference signal generated from the raster scan around the pit area. A cross section of the 2D signal measured through the maximum signal peak is plotted in Figure 1.b. The peak-to-peak value of the difference signal can be used as a parameter to infer the geometric parameters of nanostructures, for instance, the pit diameter in this case.

CFS, as an optical system with multiple lens elements, inevitably experiences optical aberrations that can influence these measurements. Aberrations can alter the Fourier plane distributions distorting the two-dimensional difference signal map, and reducing the peak-to-peak signal magnitude. Therefore, a quantitative assessment of CFS performance requires evaluating the impact of controlled aberrations. The subsequent sections first introduce Zernike polynomials as a formalism for wavefront error characterization and then describe an experimental apparatus for imposing and measuring known aberrations.

## 3. ZERNIKE POLYNOMIALS

Zernike polynomials form a complete set of orthogonal functions commonly used to describe aberrations in optical systems. In theory, any general wavefront defined on a circular pupil can be decomposed in terms of Zernike polynomials as,[10]

$$W(\rho,\varphi) = \sum_{nm} C_n^m Z_n^m(\rho,\varphi) \tag{1}$$

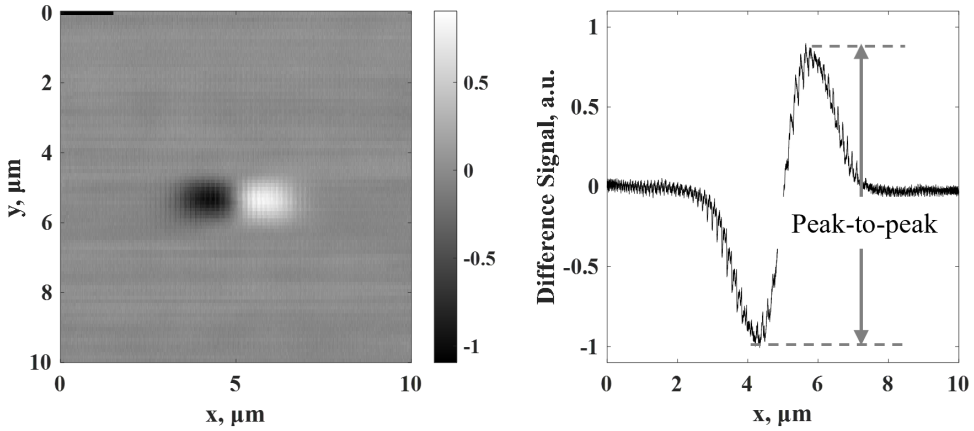


Figure 1. CFS difference signal measured using a 0.4 NA objective with laser of 632.8 nm wavelength: a) 2D scan of 10 µm x 10 µm area, b) cross section of the 2D plot shown in dashed line. The sample used for measurement consisted of a pit of 425 nm diameter and 150 nm depth etched in Si.

where, $C_n^m$ is the coefficient corresponding to each Zernike polynomial $Z_n^m$ in the decomposition of the general wavefront $W$. Following this definition, each $C_n^m$ coefficient gives the peak-valley (PV) wavefront error of the corresponding polynomial. Zernike polynomials are defined in a unit circle with $0 \leq \rho \leq 1$, $0 \leq \varphi \leq 2\pi$ and

$$Z_n^m(\rho,\varphi) = R_n^m(\rho) \cdot \left\{ \begin{array}{ll} \cos m\varphi & m \geq 0 \\ \sin m\varphi & m < 0 \end{array} \right\} \tag{2}$$

The radial function $R_n^m(\rho)$ is defined as,

$$R_n^m(\rho) = \sum_{k=0}^{(n-m)/2} (-1)^k \frac{(n-k)!}{k!(\frac{n+m}{2}-k)!(\frac{n-m}{2}-k)!} \rho^{n-2k}. \tag{3}$$

where, $n = 0, 1, 2$, etc. is the radial index and $m = -n, -n+2, ..., n-2, n$ is the azimuthal index. In this study, we limit our focus to low-order aberrations: defocus ($Z_2^0$), astigmatism ($Z_2^2$), oblique astigmatism ($Z_2^{-2}$), horizontal coma ($Z_3^1$), vertical coma ($Z_3^{-1}$), and spherical ($Z_4^0$) aberrations. Figure 2 shows the different Zernike aberrations (each with 0.4$\lambda$ PV error) alongside their corresponding focal-plane intensity patterns, calculated using the Richards–Wolf vectorial diffraction integral.[11]

## 4. EXPERIMENTAL SETUP

The influence of individual aberrations on the CFS scan signal was studied by introducing controlled amounts of each aberration into the Fourier plane of the objective using an SLM. The modified CFS setup, including the SLM (Holoeye Pluto VIS), is shown in Figure 3.

The experimental setup consists of a HeNe laser followed by a beam expander constructed using lenses L1 ($f = 10$ mm) and L2 ($f = 250$ mm) forming a telescopic system. The expanded beam is then incident on the SLM for phase modulation. The modified wavefront is relayed to the back focal plane of the objective (Leica, N PLAN L 20x/0,40 NA) using another telescope system formed using lenses L3 ($f = 200$ mm) and L4 ($f = 250$ mm). The objective focuses the light on the sample and collect the scattered field. The field in the back focal plane after reflection is relayed to the differential detector (SD 113-24-21-02) and camera using telescopic pairs L5-L6 ($f = 40$ mm) and L5-L7 ($f = 50$ mm). A flipping mirror is used to switch the beam path between the detector and camera.

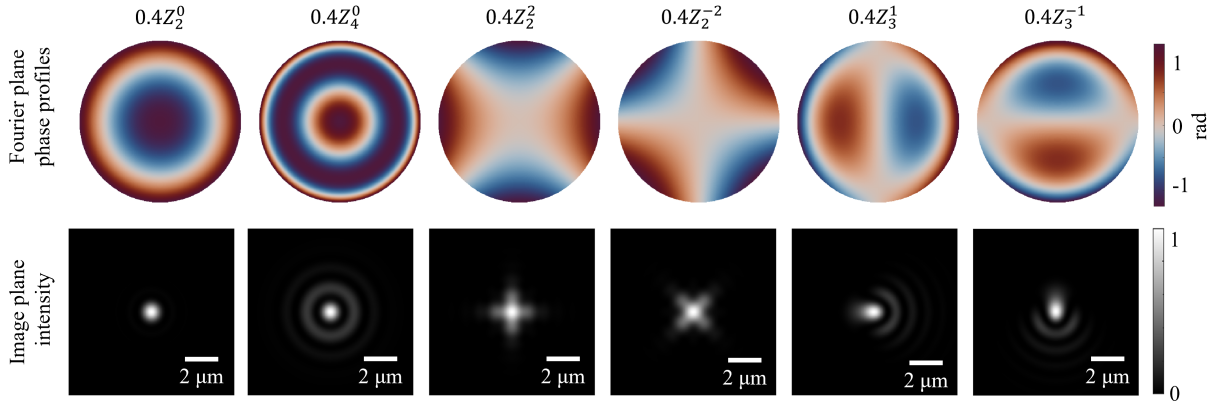


Figure 2. Theoretical point spread functions of 0.4 NA focusing system with different Zernike aberrations along with the input phase distribution in the Fourier plane. The field is polarised along the $x$-direction in the Fourier plane. The coefficients correspond to PV error for each wavefront.

In this configuration, a beam splitter is used to separate the incident and reflected beams from the SLM while ensuring that the beam is incident normally on the SLM. Although this approach results in greater laser power loss compared to positioning the SLM at a small angle to separate the incident and reflected beams, it simplifies the process of applying and projecting aberrations. The power incident on the sample is 85 µW.

The sample is mounted on a stack of piezo stages: an $x$-$y$ translator (P-625.2 CD, Physike Instrument) for 2D raster scanning and a $z$-piezo (PI-753.3, Physik Instrumente) for fine focus adjustments. The piezo stages have different in-built sensors that can provide positional information for feedback. These feedback signals are used to assign $x$ and $y$ coordinate information to the difference signal, enabling us to create a 2D differential scattering map. The difference signal along with the feedback signals are recorded using an ADC (NI 5734, National Instruments).

## 5. RESULTS

In this section we discuss the influence of different aberrations on the CFS difference signal. This was studied by individually varying the coefficient of each aberration between -1 to 1. The coefficient with an absolute value of 1 corresponds to a PV wavefront error of $\lambda$. The aberrated focused spot is then raster scanned across a sample with known geometric parameters, and the changes to the scattered signal is studied.

### 5.1 Difference signal

The point spread function (PSF) of an optical system defines the response of the system to a point source. In microscopy systems, it is common practice to use fluorescent microspheres embedded in a homogenous medium to estimate the PSF experimentally.[12] Similarly, the 2D difference signal of the CFS system when measuring a sub-wavelength scatterer can give an estimate of the optical response of the system. The differential maps does not correspond exactly to the PSF but does provide a good approximation for qualitative analysis. The sample used in this case consists of pits of 425 nm diameter and 150 nm depth etched into Silicon. The theoretical size of an unaberrated focused spot of 0.4 NA is 1.93 µm.[13]

Figure 4 shows the normalised 2D difference scan signals of a single etched pit when scanned with focused spots of different aberrations. The third row (a.3 - e.3)) shows the measurements when the sample is in the $z$-plane with the maximum peak-to-peak of the difference signal. The first, second and fourth rows correspond to measurements from $z$-planes at distances of $-5$ µm, $-2$ µm and 2 µm from the maximum peak-to-peak signal plane respectively. Each column corresponds to a distinct aberration: a) defocus ($Z_2^0$) /no aberration added, b) spherical ($Z_4^0$), c) astigmatism ($Z_2^2$), d) oblique astigmatism ($Z_2^{-2}$), and e) vertical coma ($Z_3^{-1}$).

The scans looks similar to the familiar aberrated PSFs in lensed optical systems. For the astigmatic spot, the difference signal is elongated along the horizontal in the $z = -2$ µm plane and along the vertical in $z = 2$ µm

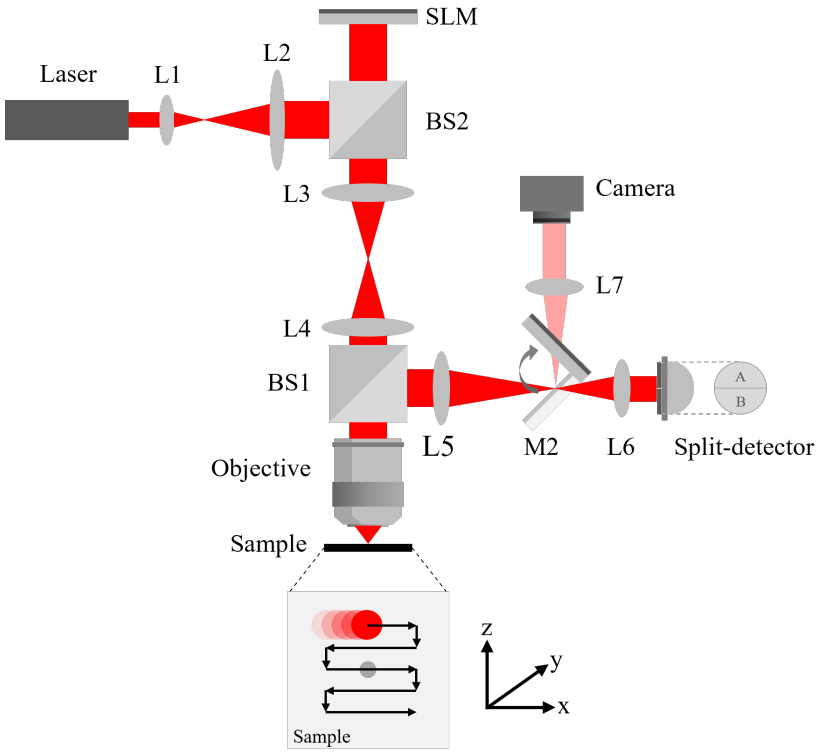


Figure 3. Schematic of the CFS setup including the SLM for calibration. Lenses L1 - 10 mm, L2 - 250 mm, L3 - 200 mm, L4 - 250 mm, L5 - 200 mm, L6 - 40 mm, L7 - 50 mm, beam splitters - BS1, BS2, Obj - 0.4 NA objective lens, M1 - flipping mirror, SLM - spatial light modulator (Holoeye Pluto VIS). The system uses a HeNe laser with 632.8 nm wavelength.

plane. The orientation of the lobes in the difference signal gets rotated by $\pm 45°$ with respect to the scanning direction ($x$-axis in this case) in presence of oblique astigmatism. Further, the lobes get stretched along $\pm 45°$ along the different $z$-directions.

For defocus, spherical, oblique astigmatism and vertical coma aberrations, the width of the scan signal is smaller in the $z = -2\,\mu m$ plane compared to the $z = 0\,\mu m$ plane. However, further away from the $z = -2\,\mu m$ plane, the signal spreads out again. In case of the spherical and coma aberrations, there are additional ring structures around the central lobes but their visibility is limited by the SNR. The response from the horizontal coma aberration is similar to that of the vertical coma but rotated by 90°.

### 5.1.1 Difference signal peak-to-peak

For a lot of applications, the peak-to-peak value of the difference signal is used as the measurand to characterise the geometrical parameters of nanostructures, for instance, the diameter of particle contaminant on a Si wafer. It is therefore important to study the effect of different aberrations on the peak-to-peak value of the difference signal. For this purpose, each aberration coefficient was varied between between a peak-to-valley error $-1\lambda$ to $1\lambda$ and the peak-to-peak signal from the resulting scan signal is measured. The sample consists of an array of pits of 425 nm diameter and 150 nm depth etched in Silicon. Figure 5 shows the peak-to-peak of the difference signal as a function of the different aberrations. Each data point is a an average across 5 different measurements.

It is evident from the plots that the influence varies across different aberrations. The influence of each aberration can be quantified as the amount or coefficient of each aberration that reduces the peak-to-peak of the difference signal by 50%. Defocus aberration has the strongest influence (PV - $0.27\lambda$), followed by spherical (PV - $0.321\lambda$) and horizontal coma aberration (PV - $0.403\lambda$). The oblique astigmatism has the least influence requiring an aberration coefficient of 0.624 for the signal to reduce to half. In practice, defocus is also the most easily correctable aberration if the sample is mounted on a $z$-adjustable stage. For a similar drop of 50%, it was

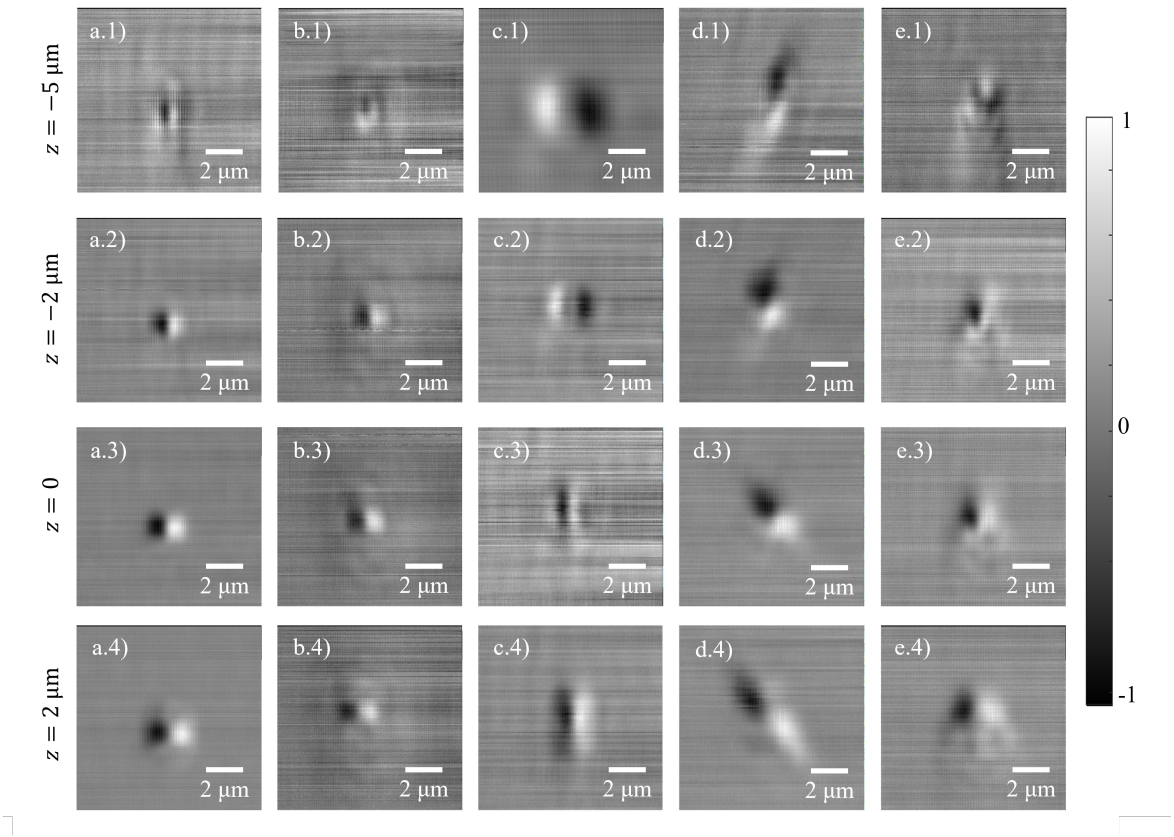


Figure 4. Optical response of the CFS signal to a sub-wavelength scatterer. The figure shows the 2D scan of a pit of 425 nm diameter etched on Si substrate with etch depth of 150 nm. The scans were made using a focused spot at 633 nm wavelength generated using an 0.4 NA objective. Each column corresponds to the response of the system with a specific aberration, with each row corresponding a different focal plane. a.1 - a.4 no aberrations added, b.1 - b.4 1$\lambda$ spherical aberration, c.1 - c.4 0.8$\lambda$ astigmatism, d.1 - d.4 0.8$\lambda$ oblique astigmatism and e.1 - e.4 1$\lambda$ vertical coma.

experimentally measured that the sample has to be moved by 3.75 µm from the plane with the largest signal peak-to-peak along the $z$-direction.

The peak-to-peak distributions are characteristic of the specific optical components of the system and may differ depending on the design of the objective and other lens elements. Similar plots when using a 0.9 objective lens is shown in Appendix A.

## 6. DISCUSSION

In this study, we have comprehensively analysed the effects of various optical aberrations on coherent Fourier scatterometry (CFS) signals. Using Zernike polynomials to systematically characterise these aberrations, controlled wavefront errors were introduced into a CFS setup via an SLM. The resulting 2D differential scan maps demonstrated that the influence of optical aberrations on the optical response of the CFS system to a point-like scatterer is similar to their effects in microscopy. Specifically, defocus aberration consistently broadened the signal away from the focal plane, while astigmatism and oblique astigmatism elongated the signal along orthogonal axes. Spherical and coma aberrations introduced additional ring structures around the central scattering signal. We further quantified the impact of these aberrations by examining their influence on the peak-to-peak amplitude of the differential signals. Among the tested aberrations, defocus had the most significant impact, followed closely by spherical and coma aberrations. In contrast, oblique astigmatism exhibited the least effect on the signal amplitude. However, defocus aberration is also the easiest to correct through axial adjustment.

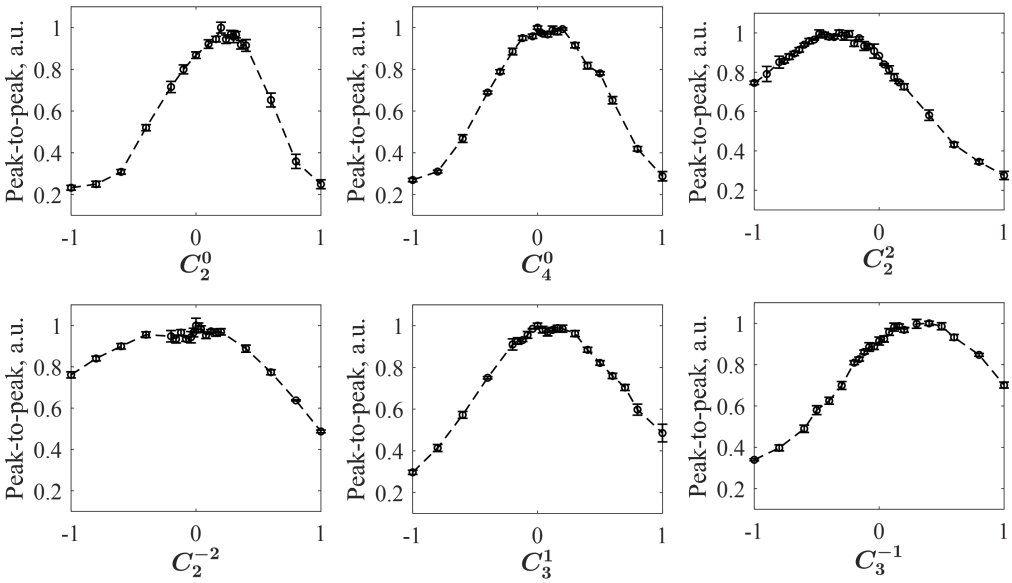


Figure 5. The variation in peak-to-peak of the differential signal as a function of aberration coefficients for a) defocus ($Z_2^0$), b) spherical ($Z_4^0$), c) astigmatism ($Z_2^2$), d) oblique astigmatism ($Z_2^{-2}$), e) horizontal coma ($Z_3^1$), f) vertical coma ($Z_3^{-1}$). The sample consists of a pit of 425 nm diameter and 150 depth etched in Si. The system uses an NA of 0.4 and wavelength of 632.8 nm. The coefficients were varied between $\pm 1\lambda$.

Understanding how these aberrations influence CFS performance is crucial not only for understanding the performance of current CFS systems but also for designing future setups. For example, substituting piezo stages with beam-scanning galvo mirrors for high-throughput scanning, could introduce significant astigmatism and coma aberrations, affecting overall system performance. The current study can be used to determine the range of scan angles that can be used without significantly affecting the performance of the system. The findings from our study thus serve a dual purpose: providing essential insights into the fundamental behaviour of optical aberrations in CFS, and offering practical guidelines for new system design parameters.

## APPENDIX A. 0.9 NA OBJECTIVE

Figure 6 shows the influence of different aberrations on the the peak-to-peak of the difference signal obtained from the split-detector for a 0.9 NA system. The aberration coefficient for each aberration is varied such that the PV is between $\pm 1\lambda$. The sample consists of a pit with 425 nm diameter and 150 nm depth etched in Si. The influence of different aberrations seems comparable to the 0.4 NA objective.

## ACKNOWLEDGMENTS

We acknowledge the Nederlandse Organisatie voor Wetenschappelijk Onderzoek (Project 17-24 Synoptics No. 2) for funding this research. We also thank Luuk Zonneveld from TU Delft for the software used to control the SLM. We acknowledge the use of AI-assisted tools, including language and grammar checking software, to improve the clarity and readability of the manuscript.

## REFERENCES

[1] Fernández Herrero, A., Scholze, F., and Dai, G. e. a., "Analysis of line-edge roughness using euv scatterometry," *Nanomanufacturing and Metrology* **5**, 149–58 (2022).

[2] Diebold, A. C., Antonelli, A., and Keller, N., "Perspective: Optical measurement of feature dimensions and shapes by scatterometry," *APL Materials* **6**, 058201 (05 2018).

[3] Whitworth, G. L., Francone, A., Sotomayor-Torres, C. M., and Kehagias, N., "Real-time optical dimensional metrology via diffractometry for nanofabrication," *Scientific Reports* **10**(5371) (2020).

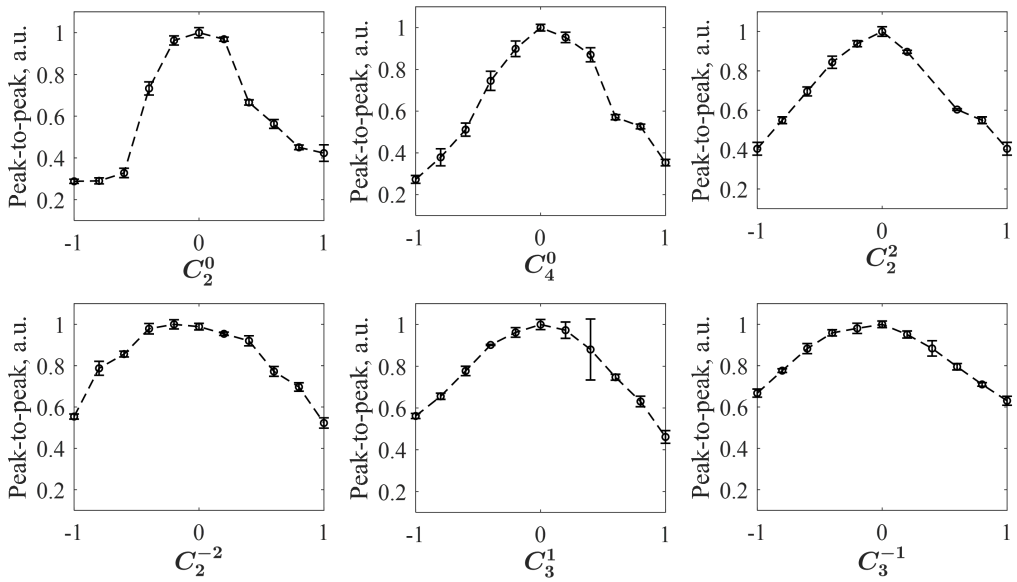


Figure 6. The variation in peak-to-peak of 0.9 NA CFS difference signal as a function of aberration coefficients for a) defocus ($Z_2^0$), b) spherical ($Z_4^0$), c) astigmatism ($Z_2^2$), d) oblique astigmatism ($Z_2^{-2}$), e) horizontal coma ($Z_3^1$), f) vertical coma ($Z_3^{-1}$). The sample consists of a pit of 425 nm diameter and 150 depth etched in Si.


[4] Huang, H.-T. and Terry Jr, F. L., "Spectroscopic ellipsometry and reflectometry from gratings (scatterometry) for critical dimension measurement and in situ, real-time process monitoring," *Thin Solid Films* **455-456**, 828–836 (2004). The 3rd International Conference on Spectroscopic Ellipsometry.

[5] Roy, S., Bouwens, M., Wei, L., Pereira, S. F., Urbach, H. P., and van der Walle, P., "High speed low power optical detection of sub-wavelength scatterer," *Review of Scientific Instruments* **86**(12), 123111 (2015).

[6] Kumar, N., Petrik, P., Ramanandan, G. K. P., Gawhary, O. E., Roy, S., Pereira, S. F., Coene, W. M. J., and Urbach, H. P., "Reconstruction of sub-wavelength features and nano-positioning of gratings using coherent Fourier scatterometry," *Opt. Express* **22**(20), 24678–24688 (2014).

[7] Menzel, M. and Pereira, S. F., "Coherent Fourier scatterometry reveals nerve fiber crossings in the brain," *Biomed. Opt. Express* **11**(8), 4735–4758 (2020).

[8] Rafighdoost, J., Kolenov, D., and Pereira, S. F., "Coherent Fourier scatterometry for detection of killer defects on Silicon carbide samples," *IEEE Transactions on Semiconductor Manufacturing* **37**(1), 124–128 (2024).

[9] Roy, S., Assafrao, A. C., Pereira, S. F., and Urbach, H. P., "Coherent Fourier scatterometry for detection of nanometer-sized particles on a planar substrate surface," *Opt. Express* **22**(11), 13250–13262 (2014).

[10] ISO 21457:2008(E), "Ophthalmic optics and instruments — Reporting aberrations of the human eye," standard, International Organization for Standardization (2008).

[11] Herrera, I. and Quinto-Su, P. A., "Simple computer program to calculate arbitrary tightly focused (propagating and evanescent) vector light fields." https://arxiv.org/abs/2211.06725 (2022).

[12] Cole, R. W., Jinadasa, T., and Brown, C. M., "Measuring and interpreting point spread functions to determine confocal microscope resolution and ensure quality control," *Nature Protocols* **6**(12), 1929–1941 (2011).

[13] Goodman, J. W., [*Introduction to Fourier optics*], Roberts & Co. publishers, Greenwood village (2005).